A. Ozgurluk, K. A. Peleaux, and C. T.-C. Nguyen, "Widely tunable 20-nm-gap ruthenium metal square-plate resonator," *Tech. Digest*, 2019 IEEE Int. Micro Electromechanical Systems Conference, Seoul, Korea, Jan. 27-31, 2019, pp. 153-156, DOI: 10.1109/MEMSYS.2019.8870623.

WIDELY TUNABLE 20-NM-GAP RUTHENIUM METAL SQUARE-PLATE RESONATOR

Alper Ozgurluk, Kieran Peleaux, and Clark T.-C. Nguyen
Department of EECS, University of California at Berkeley, Berkeley, California, USA

ABSTRACT

A capacitive-gap transduced flexural-mode square-plate resonator constructed in rapid-thermal-annealed (RTA'ed) ruthenium metal posts quality factors (Q's) exceeding 5000 and an impressive transducer strength C_x/C_o (equivalent to k_t^2) of up to 71% intrinsic and 36% with 55fF of bond capacitance loading, which in turn permits more than 46% voltage-controlled resonance frequency tuning (from 18.005 to 9.713MHz) with a voltage excursion from 0.5 to 2.8V. The 36% C_x/C_o is 75 times larger than the 0.48% of published AlN piezoelectric material in this HF frequency range [1]. With processing temperatures potentially below 350°C (with localized annealing), this metal resonator is amenable to integration directly over even advanced node CMOS [2], making this technology attractive for single-chip widely tunable filter and oscillator applications, e.g., for wireless communications [3].

INTRODUCTION

Low metal material deposition temperatures have long enticed researchers seeking to integrate MEMS directly over CMOS. However, metal resonators have historically suffered from low Q relative to polysilicon or diamond counterparts [4], with metal Q's for flexural modes generally in the range of 180 [5]. Recent demonstration of a localized anneal-based method to boost the Q's of Ru metal clamped-clamped beam resonators [5] and reduce aging rates [6] are now making metal attractive once again, especially for timing and communications applications. However, for applications like the super-regenerative transceiver of [7], for which resonance frequency sets the receivable channel range, such resonators would be even more useful if their frequencies were voltage-tunable over larger ranges than the 80 kHz previously shown in [7]. This work achieves a more than 100 times increase in tuning range via use of a nano-scale square-plate resonator design with 20-nm electrode-to-resonator gaps.

DEVICE STRUCTURE AND MODEL

Fig. 1 presents the perspective view of the square-plate resonator with dimensions and in a typical bias and excitation circuit configuration. The device is similar in structure to that of [8], but differs in its use of Ru metal structural material and interconnects (as opposed to polysilicon), as well as much smaller dimensions. Here, the 3.4-µm side length, 75-nm thickness, and 20-nm electrode-to-resonator gap are much smaller than the 16-µm, 2.2-µm, and 90-nm of [8]. The inset in Fig. 1 presents the trampoline mode shape that permits larger pull-in voltages than other designs. Tensioning via annealing [5] further strengthens it against pull-in, allowing it to stay suspended even with 2.8V across its 20-nm electrode-to-resonator gap. This then enables intrinsic and loaded C_x/C_o's of 71.2% and 36.1%, respectively, that permit the described wide tuning range.

To elaborate on this, the Rayleigh-Ritz method offers a convenient approach to generate an expression for the trampoline mode shape employed here [9]. This method begins with a guess for the mode shape function Z_{mode} that satisfies the fixed boundary conditions at the four corners. For a square plate of edge size L centered at the origin, one good guess takes the form

$$Z_{mode}(x,y) = a_1\left\{2-\left(\frac{2x}{L}\right)^2-\left(\frac{2y}{L}\right)^2\right\}+a_2\left\{1-\left(\frac{2x}{L}\right)^2\left(\frac{2y}{L}\right)^2\right\} \quad (1)$$

where x and y are independent coordinate variables. a_1 and a_2 are adjustable parameters that minimize the difference between the total strain energy and work done by a point load of F applied at the center of the plate when taking values

$$a_1 = \frac{FL^2}{512D(1+\nu)}\frac{43-45\nu}{6-5\nu} \quad (2)$$

$$a_2 = \frac{15FL^2}{512D(6-5\nu)} \quad (3)$$

where ν is Poisson's ratio and D is flexural rigidity:

$$D = \frac{EH^3}{12(1-\nu^2)} \quad (4)$$

where E is Young's modulus and H is the square plate thickness. Use of (1)-(4) yields the equivalent mechanical stiffness k_m at the center of the square plate

$$k_m = \frac{128EH^3}{3L^2}\frac{6-5\nu}{(1-\nu)(101-75\nu)} \quad (5)$$

The dynamic mass referenced to the highest velocity point, i.e., the square plate center, takes the form [10]

$$m_m = \frac{\rho H \iint Z_{mode}^2\,dx\,dy}{Z_{mode}^2(x=0,y=0)} = \kappa_{sq}\rho H L^2 \quad (6)$$

where κ_{sq} is mass modification factor given as 0.559 for ruthenium with ν = 0.3. Substituting (5) and (6) in the well-known resonance frequency expression leads to

$$f_{nom} = \frac{1}{2\pi}\sqrt{\frac{k_m}{m_m}} = \frac{1}{2\pi}\frac{H}{L^2}\sqrt{\frac{E}{\rho}\frac{128}{3\kappa_{sq}}\frac{6-5\nu}{(1-\nu)(101-75\nu)}} \quad (7)$$

where ρ is density. For the device studied in this work with H = 75nm, L = 3.4µm, E = 402.5GPa, ρ = 13420kg/m^3, and ν = 0.3, (7) predicts a trampoline mode resonance frequency of 14.138MHz.

To complete the device equivalent circuit, the electromechanical coupling factor η_e referenced to the square-plate center takes the form [11]

$$\eta_e = \gamma\frac{V_P C_o}{d_o} \quad (8)$$

where V_P is the dc-bias voltage, C_o is the total electrode-to-resonator overlap capacitance, d_o is the electrode-to-resonator gap, and γ is a parameter that modifies the electromechanical coupling of an ideal parallel-plate capacitive-gap transducer to account for a non-constant resonance displacement (or velocity) profile over the electrode area [11] given by

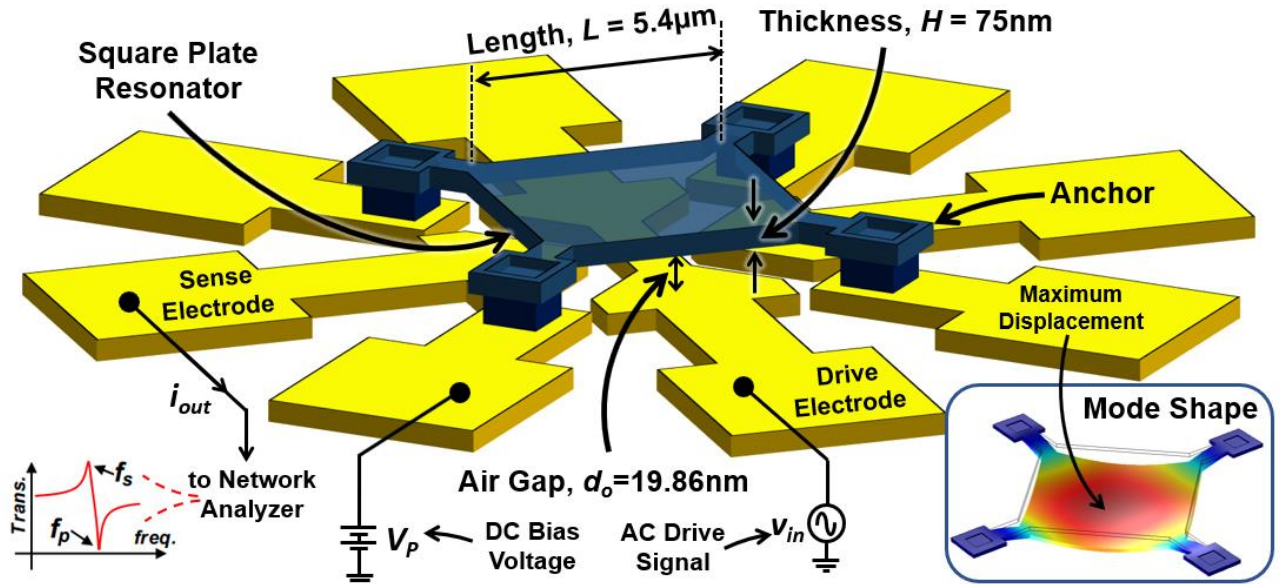

Fig. 1: The square plate device described herein in a typical operating circuit with dimensions. The inset shows the finite element analysis (FEA) simulated mode shape.

$$\gamma = \frac{1}{L^2}\frac{\iint Z_{mode}(x',y')\,dx'\,dy'}{Z_{mode}(x,y)} \qquad (9)$$

The dependence of the electromechanical coupling factor on the second power of the electrode-to-resonator gap spacing makes clear that smaller gaps can greatly increase the electromechanical coupling, as well as the electromechanical coupling strength, which takes the form

$$\frac{C_x}{C_o} = \gamma^2 V_P^2 \frac{(1-\nu)(101-75\nu)}{6-5\nu}\frac{3\varepsilon_o L^4}{128EH^3 d_o^3} \qquad (10)$$

Equation (9) together with (5)-(8) now allow specification of the device equivalent circuit in Fig. 2.

STRUCTURE-ASSISTED TUNING RANGE

Voltage-controlled resonance frequency tuning for the square-plate resonator comes about via the well-known electrical stiffness associated with any parallel-plate capacitive-gap transducer. Electrical stiffness not only renders the resonance frequency f_o a strong function of dc-bias voltage V_P, it also often sets the maximum value of V_P before

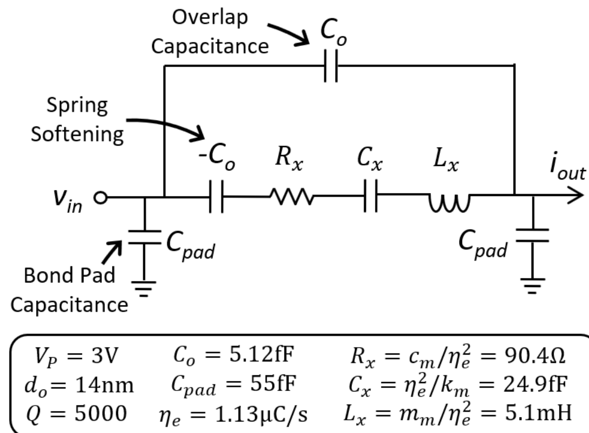

Fig. 2: Equivalent circuit for a square plate resonator operated as a one-port. Numerical values are for the device alone, i.e., with no parasitic line resistance.

the onset of device pull-in. The expression for the electrical stiffness k_e acting on the V_P-biased Fig. 1 square-plate resonator with all electrodes grounded is [11]

$$k_e = \frac{\eta_e^2}{C_o} = V_P^2\gamma^2\frac{\varepsilon_o L^2}{d_o^3} \qquad (11)$$

when taking as a reference point the maximum displacement location indicated in the trampoline mode shape in Fig. 1 inset, γ is 0.722.

This electrical stiffness acts against the resonator's mechanical stiffness to lower the resonance frequency according to

$$f_o = f_{nom}\sqrt{1-\frac{k_e}{k_m}} = f_{nom}\sqrt{1-\frac{C_x}{C_o}} \qquad (12)$$

where

$$k_m = \frac{\eta_e^2}{C_x} \qquad (13)$$

permits the rightmost form. (12) shows that k_e/k_m is the same as the intrinsic, i.e., no parasitics, C_x/C_o of the resonator. Thus, the higher the C_x/C_o, the larger the frequency tuning range. From (10) and (12), the 20-nm initial electrode-to-resonator gap of this work contributes to a large C_x/C_o and correspondingly large frequency tuning range.

The smaller stiffness of this nano-scale square-plate device enhances the frequency tuning range not only by increasing the k_e/k_m term in (12), but also by allowing the increasing dc-bias voltage to pull the device closer to its underlying electrode. In particular, unlike much stiffer devices with small gaps, e.g., the 13-nm-gap wine-glass disk of [12], this trampoline-mode square-plate device under 2.8V dc-bias bends significantly under the attractive force, reducing the original 20-nm gap by 33% at the plate center and increasing C_x/C_o accordingly (to 71%)!

Fortunately, as described in [5], the rapid-thermal anneal treatment given to this device not only raises its Q, but

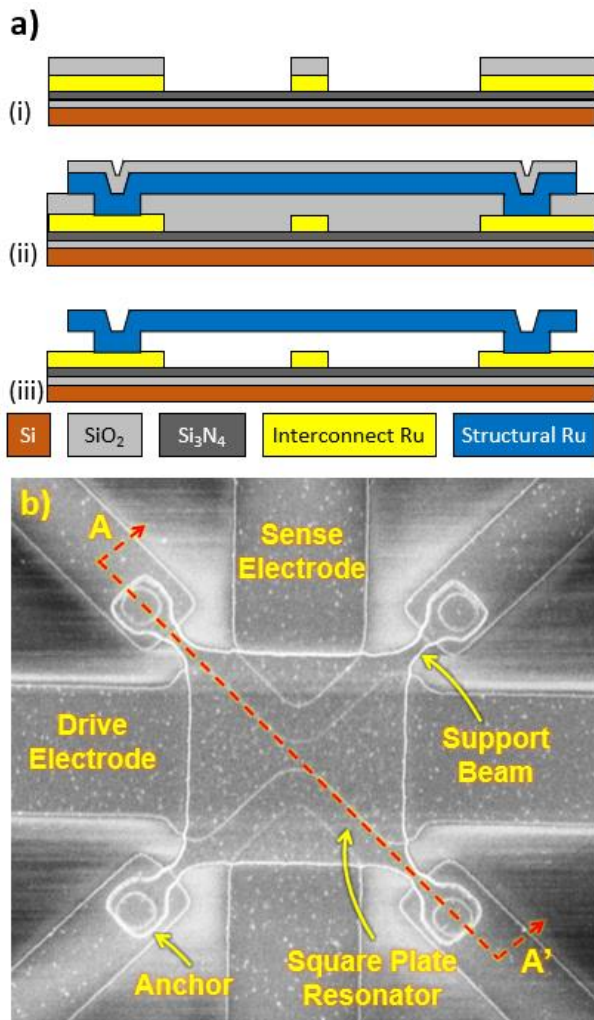

Fig. 3: a) Cross-sections through AA' after (i) interconnect layer etch (ii) structural layer etch (iii) HF release. b) SEM of a fabricated ruthenium metal square plate.

also generates tensile stress that tightens its stiffness somewhat, allowing it to stay suspended even at the 2.8V dc-bias voltage of maximum frequency tuning. At higher voltages, the device pulls in.

FABRICATION

The metal surface micromachining fabrication process for ruthenium square-plate resonators was similar to that for previous clamped-clamped beams [5], except for use of a much smaller SiO_2 sacrificial spacer layer to achieve 20-nm initial electrode-to-resonator gaps. Fig. 3(a) presents cross-sections summarizing this process, showing the use of ruthenium for both the structure and its electrodes and silicon dioxide as the sacrificial layer and as a hard mask for precise lithography and etching. Fig. 3(b) presents the SEM of a freshly fabricated square plate resonator, indicating important structural and design details.

Instead of the post-fabrication localized annealing used in [5], the square plates experienced conventional rapid-thermal annealing (RTA) at 850°C for 180 seconds with 30-second temperature rise and fall times. This was a time-saving measure that (as will be seen) ended up as effective in raising device Q's. Whether this would be acceptable as a post-CMOS step is yet to be seen. If not, then localized annealing is always an option.

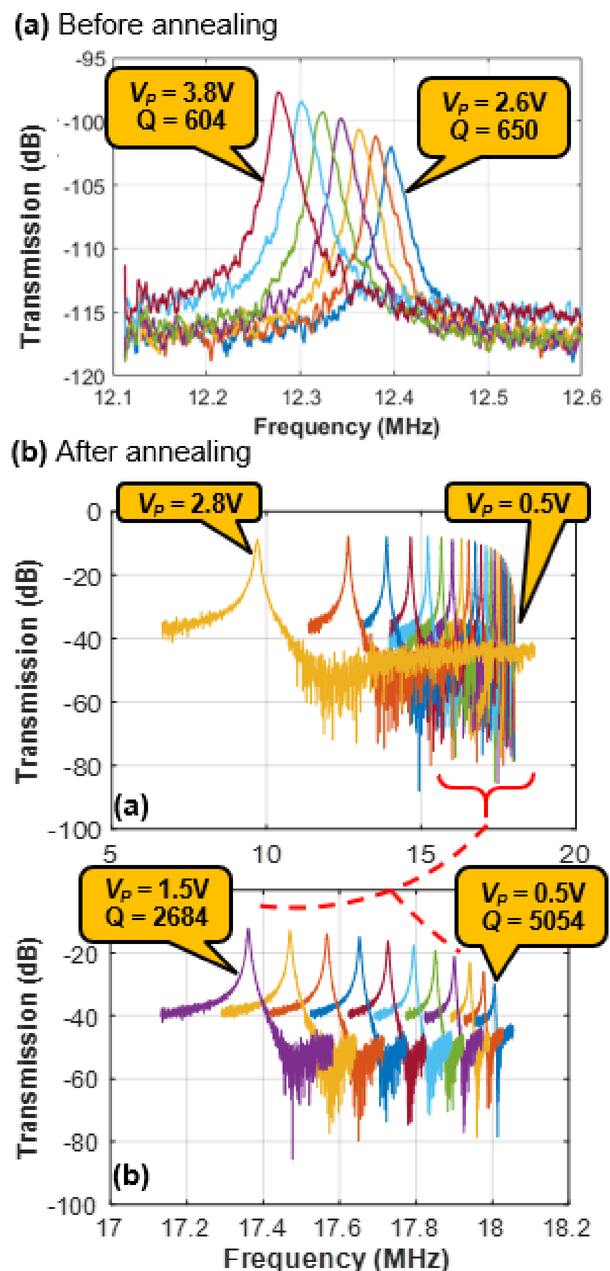

Fig. 4: Measured frequency spectra for a ruthenium metal square plate resonator as a function of dc-bias voltage (a) before RTA using mixing V_{LO} = 1V_{pp}, f_{LO} = 6MHz, P_{RF} = -3dBm [14] (b) after RTA using direct measurement.

EXPERIMENTAL RESULTS

A Lakeshore FWPX Vacuum Probe Station housed and electrically accessed Ru square-plate devices during measurement. Fig. 4 (a) and (b) present vacuum-measured transmission spectra before and after annealing, respectively, clearly showing both a frequency shift and an increase in Q. In particular, fabricated Ru square-plate devices posted Q's in the range of only 600 before RTA. After RTA, their Q's rose to over 5000 at a dc-bias of 0.5V. RTA also permits a much wider frequency tuning range, from 18.005 to 9.713MHz over 0.5 to 2.8V—a 46% range. Needless to say, this is an astonishing range of frequency not often (if ever) seen in a resonator with such a high Q.

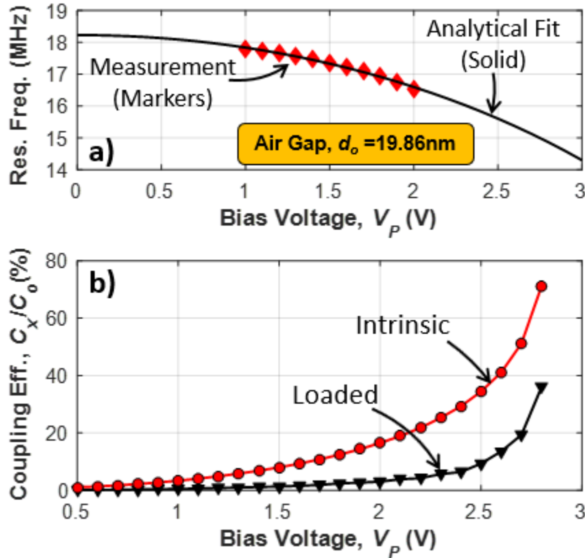

Fig. 5: a) Measured frequency versus dc-bias voltage with curve-fit to extract electrode-to-resonator gap. b) Intrinsic and loaded C_x/C_o versus dc-bias voltage.

The larger RTA'ed tuning range likely results from tensioning that flattens the square plate, bringing it closer to its electrode than an un-annealed counterpart.

A curve fit of the plot of resonance frequency versus dc-bias in Fig. 5(a) with electrical stiffness theory [13] confirms an initial electrode-to-resonator gap spacing of 21.95nm at V_P=1V and a final spacing of 14.69nm at the highest applied V_P=2.8V. The very fast change in frequency with dc-bias on the left side of the plot confirms the role of gap reduction as the square plate bends closer to the electrodes under the large (μN-range) attractive force.

Since from (12) the intrinsic (i.e., unloaded) C_x/C_o essentially equals k_e/k_m, another curve fit also yields the plot of intrinsic (i.e., unloaded) C_x/C_o versus dc-bias in Fig. 5(b), where 2.8V yields a whopping 71.2%!

The practical C_x/C_o is not this large, as it suffers somewhat from loading by parasitic capacitance. In particular, in any real situation parasitic capacitance (in the leads, measurement circuit, etc.) adds to the C_o in C_x/C_o, lowering its actual value. The common approach to attaining C_x/C_o via measurement of parallel and series resonance frequencies, f_p and f_s (indicated in Fig. 1), respectively, then using

$$\frac{C_x}{C_o} = 1 - \left(\frac{f_s}{f_p}\right)^2 \qquad (14)$$

in fact yields the loaded C_x/C_o.

Fig. 5(b) uses (14) to also plot the loaded C_x/C_o versus V_P, which now sports a still-impressive value of 36.1% at V_P = 2.8V. While C_x/C_o rises with dc-bias, the Q drops due to loading by parasitic interconnect resistance, which is comparable to the motional resistance at high dc-bias, e.g., motional resistance R_x=486Ω at 2.1V. Nevertheless, the device still achieves large intrinsic and loaded (C_x/C_o)-Q products of 274 and 56 at V_P = 2.1V.

CONCLUSIONS

Many who work with high Q resonators, practitioners and researchers alike, are familiar with the adage that high Q resonators are simply not tunable, meaning that some other means to realize tuning, e.g., phase-locking to a (dirty) voltage-controlled oscillator, is necessary. The resonator of this work challenges this assumption and could be a potential game-changer for many applications that benefit from frequency tuning, including tunable oscillators and filtering for RF front-ends. The benefits of this go over and beyond the already important benefit of CMOS-compatibility, which this high-Q ruthenium structural material achieves when localized annealed [5].

Aside from tuning, note that all of the measured values—Q, C_x/C_o, tuning range, k_t^2-Q—are not only impressive for CMOS-compatible metal material, but also better than or competitive with other common micromachinable resonator materials in this frequency range, including polysilicon, diamond, and AlN. Whether they can also compete from a stability perspective, especially long-term stability, remains to be seen.

ACKNOWLEDGMENT

We thank the DARPA N-ZERO program for initial support for this work.

REFERENCES

[1] G. Piazza et al., "Piezoelectric Aluminum Nitride Vibrating Contour-Mode …," DOI: 10.1109/JMEMS.2006.889503.

[2] E. P. Gusev et al., "Advanced high-κ dielectric stacks …," DOI: 10.1147/rd.504.0387

[3] A. Ozgurluk et al., "RF Channel-Select Micromech…," DOI: 10.1109/TUFFC.2018.2881727

[4] W.-L. Huang et al., "Fully monolithic CMOS …," DOI: 10.1109/MEMSYS.2008.4443580.

[5] A. Ozgurluk et al., "Q-boosting of metal MEMS …," DOI: 10.1109/FCS.2017.8088786.

[6] W.-T. Hsu et al., "In situ localized …," Transducers 1999.

[7] T. O. Rocheleau et al., "A MEMS-based RF channel-selecting …," Hilton Head 2014.

[8] M. U. Demirci et al., "Mechanically corner-coupled square …," DOI: 10.1109/JMEMS.2006.883588.

[9] S. Timoshenko, Vibration Problems in Engineering, 4th Ed., New York: Wiley, 1974.

[10] R. Johnson, Mechanical filters in electronics, Wiley, 1983.

[11] M. Akgul et al., "A negative-capacitance equivalent circuit model…," DOI:10.1109/TUFFC.2014.2976.

[12] J. N. Nilchi et al., "High Cx/Co 13nm-capacitive-gap transduced …," DOI:10.1109/MEMSYS.2017.7863560.

[13] W.-T. Hsu et al., "Stiffness-compensated temperature-insensitive …," DOI: 10.1109/MEMSYS.2002.984374.

CONTACT

*A. Ozgurluk, tel:+1-510-7016897; ozgurluk@berkeley.edu